MSDE

PAPER

View Article Online
View Journal

Cite this: DOI: 10.1039/d6me00015k

Tuning zwitterionic polymer interactions with water and ice through side-chain engineering

Tamalika Ash, [a] Sara A. Tolba [bc] and Wenjie Xia *[a]

Ice formation on solid surfaces presents major engineering challenges. Although zwitterionic polymer coatings show promising anti-icing performance, the fundamental role of the side-chain carbon spacer in governing polymer–water and polymer–ice interactions remains insufficiently understood. Here, density functional theory (DFT) calculations were used to investigate how the spacer length between zwitterionic groups affects these interactions, focusing on poly(2-methacryloyloxyethyl phosphorylcholine) (pMPC), a known anti-icing and anti-fouling polymer model system. To guide molecular design, the $-CH_2-$ spacer length was systematically varied to generate five representative polymers: pMPC-1, pMPC, pMPC+1, pMPC +2, and pMPC+3, with one, two, three, four, and five $-CH_2-$ units between the zwitterionic moieties, respectively. A comprehensive evaluation of polymer–water interactions, spanning the electronic structure, side-chain conformations governing water accessibility, the number and strength of bound water molecules, adsorption energetics, and charge transfer, was performed to elucidate how spacer-length-dependent molecular features control hydration. These analyses show that pMPC+1 and pMPC+2, containing three- and four-carbon spacers, respectively, exhibit the most favorable hydration behavior by achieving an optimal balance between side-chain flexibility and crumpling, which enables both strong and sufficiently abundant water binding. Interaction analysis with ice clusters further indicates that pMPC+1 provides the best anti-icing performance, displaying the greatest resistance to ice formation and thereby promoting the retention of water in the liquid state. Overall, these molecular-level insights underscore the critical role of carbon spacer architecture in dictating polymer–water/ice interactions, offering valuable guidance for designing zwitterionic polymeric materials *via* side-chain engineering.

Received 25th January 2026,
Accepted 5th March 2026

DOI: 10.1039/d6me00015k

rsc.li/molecular-engineering

Design, System, Application

This study develops a molecular design approach for zwitterionic polymers by systematically tuning the carbon spacer length between oppositely charged moieties to regulate interactions with water and ice. The design strategy uses side-chain engineering as a targeted and chemically minimal means to control hydration strength, charge redistribution, and interfacial energetics without altering the polymer backbone chemistry. The molecular system is designed to promote strong and stable hydration at polymer–water interfaces, thereby reducing interactions with ice. By identifying spacer-length regimes that balance robust water binding with diminished ice affinity, the work establishes transferable molecular design principles rather than system-specific optimization. These insights enable the rational development of zwitterionic materials for anti-icing coatings and can be extended to broader hydration-controlled applications, including antifouling surfaces, membrane technologies, and biointerfaces, where controlled water–polymer interactions are critical.

Introduction

Ice formation and accumulation on solid surfaces at sub-zero temperatures present serious challenges for power transmission lines, wind turbines, telecommunication systems, and both air and ground transportation, leading to structural and functional performance issues and increasing the risk of severe accidents.[1–6] Conventional deicing strategies such as applying salt or glycol-based fluids[7] or the use of sacrificial coatings like silicone grease[8,9] have notable drawbacks, including the need for frequent reapplication, high costs, and detrimental environmental impacts. As an alternative, icephobic[10,11] and anti-icing[11,12] surfaces have drawn interest, but the intricate mechanisms behind icephobicity continue to hinder the design of reliable ice-repellent materials. Recent studies have shown that charged surfaces and the presence of ions are crucial factors in inhibiting and delaying ice formation.[12–14]

[a] Department of Aerospace Engineering, Iowa State University, Ames, IA, 50011, USA. E-mail: wxia@iastate.edu
[b] Materials and Nanotechnology, North Dakota State University, Fargo, ND 58108, USA
[c] Center for Computationally Assisted Science and Technology, North Dakota State University, Fargo, ND 58108, USA

In this context, zwitterionic polymers, containing both positively and negatively charged groups, have attracted considerable attention as potential candidates for anti-icing applications and low ice adhesion.[15–31] Their strong hydrogen-bonding interactions with water, combined with processability, reduced environmental impact, and minimal maintenance requirements, underscore their potential for substantial cost and energy savings. Previous studies have shown that zwitterionic polymers, including poly(sulfobetaine methacrylate) (pSBMA), poly(2-methacryloyloxyethyl phosphorylcholine) (pMPC), and poly(carboxybetaine acrylamide) (pCBAA), exhibit excellent anti-icing and anti-fouling performance. For instance, Bai *et al.* developed amphiphilic coatings based on pSBMA (also called pSB), which exhibited excellent antifogging performance due to enhanced polymer–water interactions and thus retained non-freezable water.[15] Chen showed that pSBMA and pCBAA zwitterionic polymers exhibited strong hydration in aqueous environments, as revealed by sum frequency generation (SFG) vibrational spectroscopy, which prevent protein adsorption and thus leads to excellent antifouling activity.[16] Song *et al.* investigated the relationship between material composition and structural features by modeling three zwitterionic brushes with CBMA, SBMA, and MPC to elucidate their role in preventing protein adhesion using molecular dynamics (MD) simulations.[17] In our previous study, we employed density functional theory (DFT) to examine the hydration behavior of four zwitterionic polymers, pSBMA, pMPC, pCBAA, and pSBi by analyzing their intermolecular interactions with water, with particular focus on how modifications to the anionic groups and the relative orientation of cationic and anionic moieties influence their interactions with water and ice.[18] Sarker *et al.* investigated the hydration behavior of trimethylamine-*N*-oxide (TMAO) and three CBs with varying charge-separation distances, combining *ab initio* MD simulations with SFG spectroscopy to probe their anti-fouling properties.[19] Their findings indicated that the spacing between anionic and cationic moieties significantly impacts the water density within the hydration layer, consequently influencing interactions with biofoulants and therefore fouling resistance performance. In a recent study, Chen *et al.* investigated the effect of the spacer length in SB and found that three $-CH_2-$ units represent a critical length, providing optimal molecular properties with the strongest charge separation and highest hydrophilicity.[20] Since the spacer length between zwitterionic moieties is found to influence hydrophilicity and antifouling activity, it is expected to play a critical role in anti-icing performance. Understanding this structure–property relationship at a fundamental molecular level could provide valuable guidance for designing effective anti-icing polymer coatings.

The zwitterionic MPC monomer, first synthesized by Ishihara and colleagues, exhibited excellent antifouling properties but was initially effective only in resisting proteins in single-protein solutions.[23] It resembles the phospholipid head groups of cell membranes, which promote the formation of stable water layers that act as barriers against protein and cell adhesion.[24] In our previous studies, we demonstrated that pMPC exhibits robust hydration, driven by strong polymer–water interactions, as evidenced by adsorption energy, polymer-to-water charge transfer, and detailed analyses of polymer–water bonds.[25] We also showed that pMPC possesses excellent anti-icing and ice-adhesion resistance properties. In pMPC, the cationic and anionic groups are separated by two $-CH_2-$ spacers. Given its effectiveness as an anti-icing agent, investigating how variations in zwitterionic group spacing within pMPC affect interactions with water, and consequently anti-icing behavior, provides an important direction for further research.

In the present study, we investigated the effect of spacing between zwitterionic groups by systematically varying the number of $-CH_2-$ spacers in pMPC. Accordingly, five zwitterionic polymer models, pMPC-1, pMPC, pMPC+1, pMPC+2, and pMPC+3, corresponding to $-(CH_2)_n-$ with n = 1,

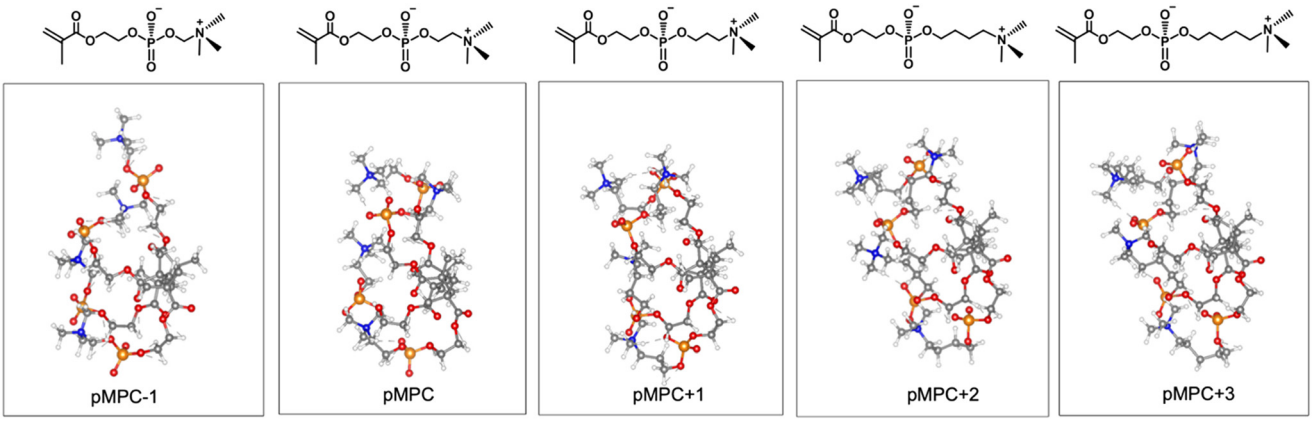

Fig. 1 Chemical structures of pMPC-1, pMPC, pMPC+1, pMPC+2 and pMPC+3 zwitterionic monomers and their corresponding optimized polymer structures.

Table 1 Electronic properties of five zwitterionic MPC monomers with different spacings

Monomer (unit)	HOMO (eV)	LUMO (eV)	Polarizability (α) (bohr^3)	Electrophilicity (ω) (eV)	Electronegativity (χ) (eV)	Dipole moment (μ) (debye)
MPC-1	−6.7	−1.3	172.9	1.5	4.0	12.7
MPC	−6.4	−1.3	184.7	1.5	3.9	14.7
MPC+1	−6.4	−1.2	195.8	1.4	3.8	14.5
MPC+2	−6.1	−1.2	207.4	1.4	3.7	15.2
MPC+3	−6.2	−1.2	220.1	1.4	3.7	14.8

2, 3, 4, 5 (Fig. 1) are considered. These polymers differ in the distance between their negatively and positively charged groups, which increases in the order: pMPC-1 < pMPC < pMPC+1 < pMPC+2 < pMPC+3. This study aims to evaluate how variations in this spacing influence interactions with water molecules and ice clusters, and consequently the polymer's anti-icing properties. We analyzed the electronic properties of the monomeric units of each zwitterionic polymer and observed that electronic properties alone cannot explain their hydration behavior. Using DFT calculations, which provide reliable predictions of electronic structures and adsorbate–adsorbent interactions, we examined the intermolecular interactions between these polymers and water. By combining multiple analytical approaches, including structural analysis, adsorption energy calculations, polymer-to-water charge transfer, and the evaluation of polymer–water bond strengths, we identified the polymers that exhibit optimal hydration. Additionally, we investigated the interactions of these polymers with a 10-H_2O-ice cluster to assess their affinity for ice. Overall, these simulations offer comprehensive insights into polymer–water and polymer–ice interactions, highlighting how variations in the carbon spacer length between zwitterionic groups can be utilized to design anti-icing coatings with improved performance. Based on our simulation results, we also proposed the optimal spacer length for preparing zwitterionic polymer coatings to get the best anti-icing performance.

Results and discussion

Electronic properties of zwitterionic polymers

We first examined the electronic properties of five zwitterionic monomers in their dry, ground-state configurations. Fig. 1 displays the chemical structures of the five zwitterionic monomers as well as their optimized polymer structures. As shown in Table 1, increasing the spacing between the cationic and anionic moieties from MPC-1 to MPC+3 results in a gradual rise in polarizability, indicating that the ease of electron cloud deformation in the presence of external agencies increases across the series. In contrast, this structural modification has a minimal impact on electrophilicity, the tendency to accept electrons, and electronegativity, the ability to attract shared electrons, both of which remain nearly constant across the series. Regarding the dipole moments, MPC-1 exhibits the lowest value (12.7 debye), while MPC+2 shows the highest value (15.2 debye); the remaining ones have dipole moments close to MPC+2.

We next calculated the density of states (DOS) for all five zwitterionic polymers, as shown in Fig. 2a. The DOS indicates the number of electronic states available per unit energy range for electron occupancy, while the Fermi level represents the highest occupied energy level at absolute zero temperature. A higher DOS intensity at the Fermi level suggests a greater number of free electrons, enhancing the polymer's potential to interact with adsorbates. Our calculations reveal that as the spacing between the cationic

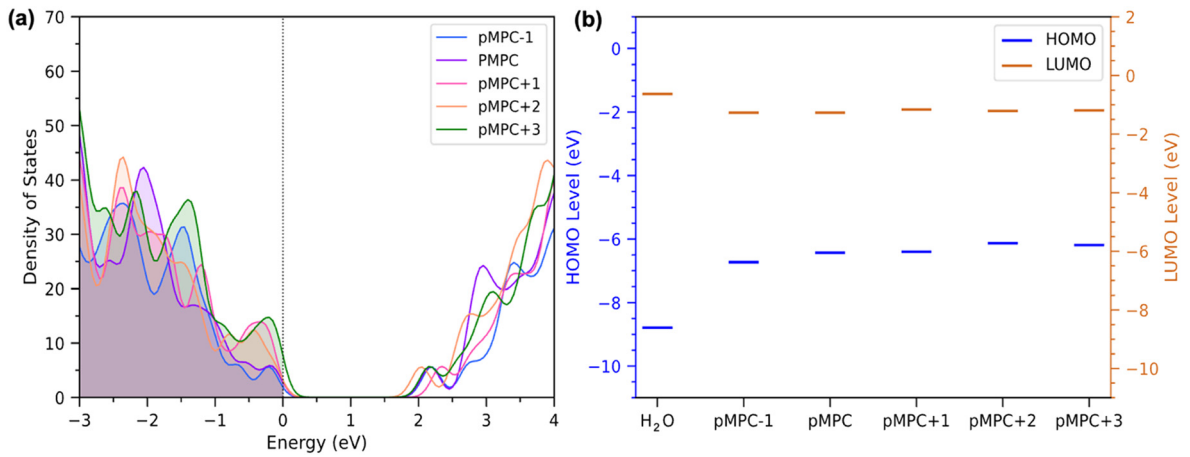

Fig. 2 Electronic properties of the five zwitterionic polymers: (a) total electronic density of states (DOS) of the polymers and (b) the calculated HOMO–LUMO energy levels of the monomers, shown alongside those of water in vacuum.

and anionic moieties decreases, the DOS intensity at the Fermi level also decreases from 7.8 states per eV for pMPC+3 to 1.9 states per eV for pMPC-1. These states primarily originate from the oxygen p orbitals, which facilitate orbital overlap with adsorbates.

We proceed to compare the HOMO–LUMO energy levels of the zwitterionic monomers with water, as shown in Fig. 2b. The calculated HOMO and LUMO energies of the monomers are energetically aligned or comparable with those of water, and the higher HOMO levels of the monomers relative to water suggest a potential for electron transfer from the polymers to water. However, the HOMO levels of all five monomers are closely aligned on a similar energy scale, indicating that none of the monomers exhibit a distinct advantage or preference for electron transfer to water. Therefore, due to the similar electronic properties of the studied zwitterionic monomers, it is difficult to determine which might exhibit stronger interactions with adsorbates, such as water solely by relying on electronic property analyses. However, based on the optimized geometries of zwitterionic polymer–water complexes and associated analyses, discussed in the following sections, we can more clearly identify which polymer exhibits the strongest interaction with water.

Conformational analysis of zwitterionic polymers under dry and wet conditions

By introducing water molecules into the system, we compared the polymer structures under dry and wet conditions. Specifically, we examined two key structural distances: the dipole–dipole distance and the side-chain distance. The dipole–dipole distance is defined as the distance between the central phosphorus (P) atom of the anionic group and the nitrogen (N) atom of the cationic group, labeled as points A and B in Fig. 3a. The side-chain distance refers to the distance between the carboxylic oxygen (O, point A) and the N atom of the cationic group (point B), as illustrated in Fig. 3b.

Our analysis shows that as the systems transition from dry to wet conditions, both dipole–dipole and side-chain distances increase. Notably, the dipole–dipole distances upon hydration increase with increasing spacing between the cationic and anionic moieties up to pMPC+2, while in pMPC +3, the average dipole–dipole distance remains comparable to that of pMPC+2. Moreover, the error bars associated with pMPC+3 under wet conditions are larger than those of the other polymers, reflecting the greater flexibility of its side chain. This flexibility arises from the longer $-CH_2-$ spacers between zwitterionic groups, which allow the side chain to fold into a loop-like structure (crumpled), stabilized by electrostatic interactions between the anionic and cationic moieties. Such folding is observed in two of the four monomeric units of pMPC+3. Because the anionic group responsible for hydrogen bonding with the water O–H is located at the middle of the side chain in these zwitterionic polymers, it allows controlled but effective interactions with water molecules. In pMPC+3, this conformational folding further restricts access of water molecules to the spatial location of the anionic sites, affecting polymer–water interactions, as shown in the analyses presented in the following sections. Finally, the overlapping error bars between dry and wet conditions suggest that some structural changes may not be statistically significant, likely due to the limited model size. Use of a larger model along with MD simulation studies could potentially reveal more pronounced effects, which might be pursued in future studies.

Water adsorption and polymer hydration

In this section, we examined the interactions between zwitterionic polymers and adsorbed water molecules, with each simulation cell containing 80 water molecules to maintain a density of approximately 0.96 g cm^{-3}. Fig. 4a–e presents the optimized ground-state geometries of the five hydrated zwitterionic polymers, together with a plot showing the average number of directly hydrogen-bonded water molecules per monomer for each polymer type (Fig. 4f). The optimized structures indicate that water molecules predominantly interact with the anionic moieties of the polymers *via* hydrogen bonding. We carefully examined each hydrated polymer to determine the number of water molecules directly interacting with the polymer. In pMPC-1,

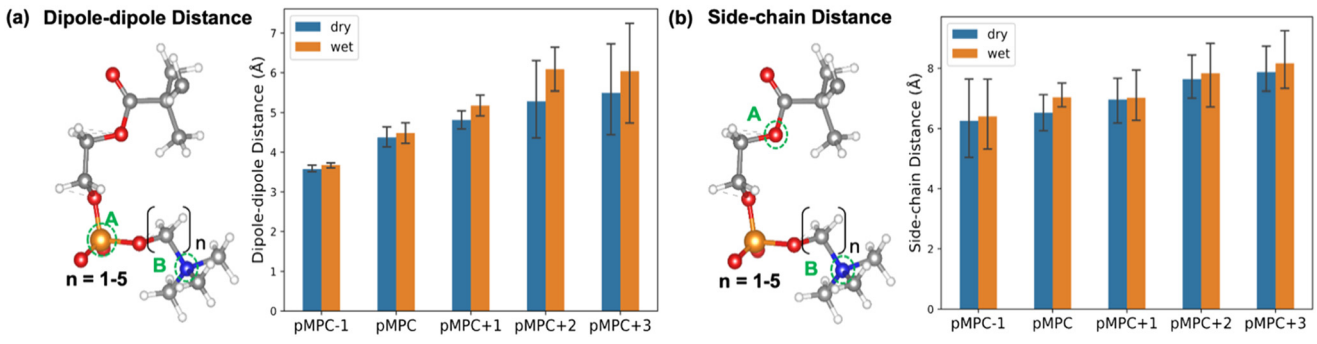

Fig. 3 Comparison of the geometric parameters of zwitterionic polymers under dry and wet conditions: (a) the schematic illustration and variation in dipole–dipole distances and (b) the schematic illustration and variation in side-chain distances.

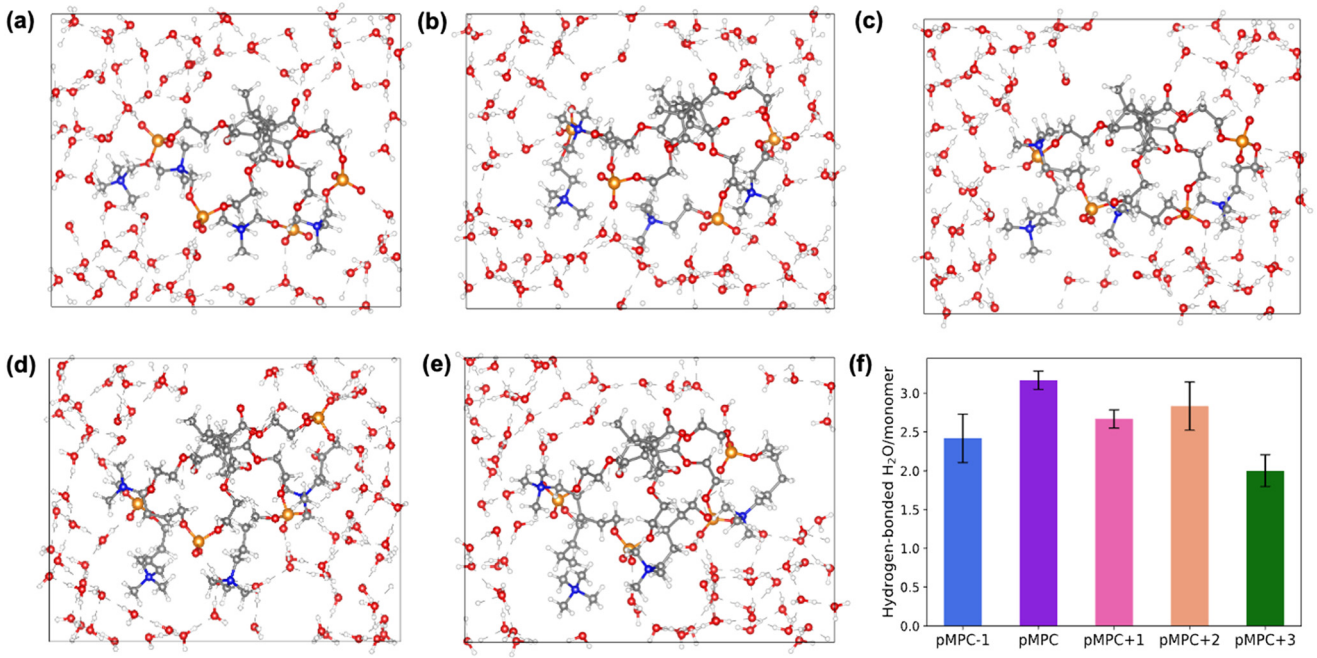

Fig. 4 Optimized ground-state geometries of all five hydrated zwitterionic polymers: (a) pMPC-1, (b) pMPC, (c) pMPC+1, (d) pMPC+2, and (e) pMPC+3 and (f) the plot of the average number of hydrogen-bonded water molecules per monomer as a function of polymer type.

an average of 2.42 water molecules form direct hydrogen bonds with the oxygen atoms of the anionic (PO_3^-) groups per monomer. For pMPC, this number is the highest, with an average of 3.17 hydrogen-bonded water molecules per monomer. pMPC+1 and pMPC+2 exhibit average values of 2.67 and 2.83 such interactions per monomer, respectively. In pMPC+3, the extent of direct hydration is the lowest, with an average of 2.00 water molecules per monomer. These variations underscore how differences in the polymer structure influence water adsorption behavior. The lower number of hydrogen-bonded water molecules in pMPC-1 is likely due to the presence of only one –CH_2– spacer between the cationic and anionic groups, which makes it behave more like a neutral polymer. pMPC, which is already established as an effective anti-icing polymer in our previous studies,[18,25] exhibits the highest number of directly bound water molecules. As the side-chain spacing increases from pMPC+1 to pMPC+3, enhanced flexibility leads to side-chain crumpling, particularly in pMPC+3, which reduces the number of accessible sites for water adsorption. For pMPC+1 and pMPC+2, a balance between chain flexibility and crumpling results in comparable levels of direct water interactions, which is more than in pMPC+3 but fewer than in pMPC. These results align well with the dipole–dipole distance analysis, which shows that even under hydrated conditions, the crumpling behavior of the polymer with the longest side chains, pMPC+3, is particularly evident in two of the four monomers. The electrostatic interaction between the anionic and cationic ends in these monomers significantly reduces the accessible surface area of the entire polymer and consequently, the number of water molecules that can directly interact with the polymer.

To gain deeper insight into the strength of polymer–water interactions and the resulting hydration behavior, we conducted three quantitative analyses: adsorption energy per water molecule (Fig. 5a), net Bader charge of H_2O molecules (Fig. 5b), and polymer–water bond strength using integrated crystal orbital Hamilton population (-ICOHP) (Fig. 5c). In this regard, it should be noted that the calculated adsorption energy includes contributions not only from polymer–water interactions but also from polymer–polymer and water–water interactions. The adsorption energy per water molecule and the net Bader charge of H_2O molecules are computed for three independent models of each polymer, and the averaged values with the corresponding error bars are presented in the plots. As shown in Fig. 5a, pMPC+1 exhibits the highest adsorption energy, followed by pMPC+2 ≈ pMPC and pMPC +3, with pMPC-1 showing the lowest. Among all five zwitterionic polymers, pMPC+2 shows the largest variation in adsorption energy across its models. The net H_2O Bader charge, defined as the sum of the charges of all 80 water molecules in the simulation cell, indicates the extent of charge transfer during adsorption (Fig. 5b). Here, pMPC shows the highest charge transfer, followed by pMPC+1 ≈ pMPC+2, then pMPC+3, while pMPC-1 exhibits the lowest. To further probe the interaction strength, we analyzed the variation of -ICOHP with polymer–water bond lengths (Fig. 5c). These results reveal that pMPC+3 forms the shortest bonds with adsorbed water molecules, with the highest -ICOHP value, indicating the strongest interaction. In contrast, pMPC shows the longest bonds, corresponding to

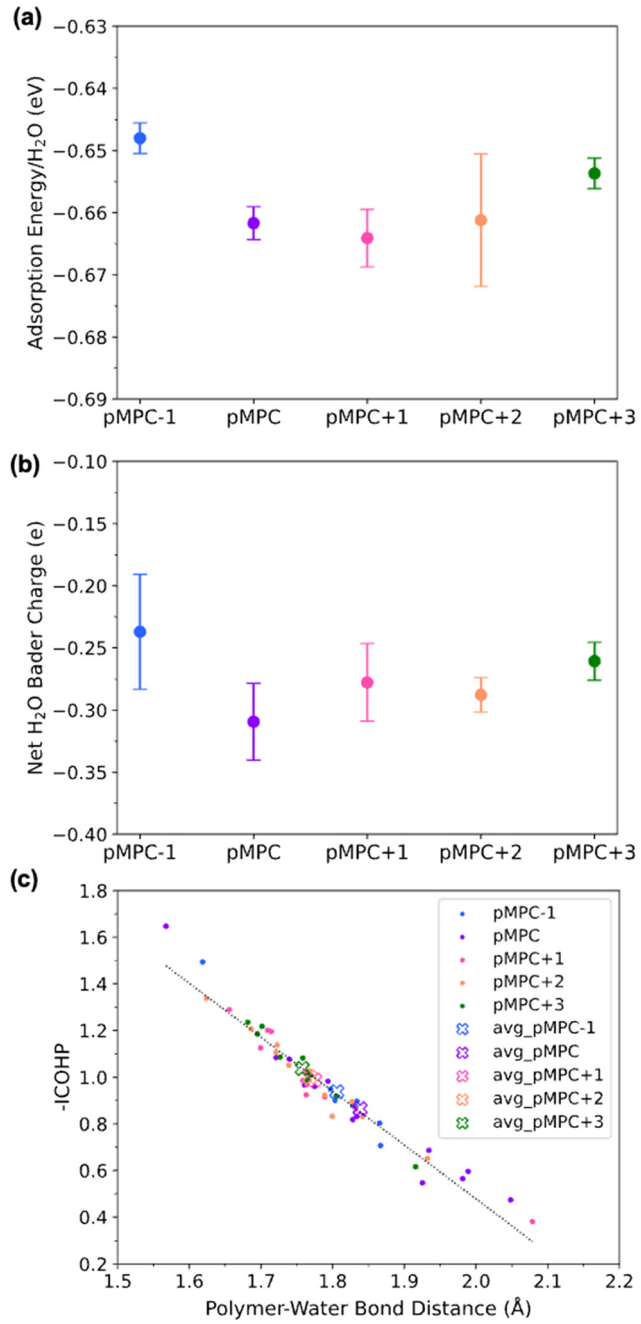

Fig. 5 (a) Water adsorption energy per water molecule, (b) net H_2O Bader charge across the materials, (c) correlation between -ICOHP and polymer–water bond lengths for pMPC-1, pMPC, pMPC+1, pMPC+2, and pMPC+3 polymers, with averaged values shown as crosses.

the weakest interaction. The bond lengths for pMPC+1 and pMPC+2 are comparable to those of pMPC+3, supporting similar strong interactions. Meanwhile, pMPC-1 exhibits intermediate bond lengths, falling between those of pMPC+1/pMPC+2 and pMPC.

While the individual analyses alone may not fully explain the hydration behavior of these polymers, taken together, they provide a more comprehensive understanding. Starting with pMPC-1, its electronic properties, the nearly unchanged dipole–dipole distance between dry and wet conditions, and the reduced number of direct water interactions collectively indicate a lower affinity for water adsorption. This is supported by its lowest adsorption energy per water molecule, lowest H_2O Bader charge, and longer, weaker polymer–water bonds, consistent with its nearly neutral character caused by a single $–CH_2–$ spacer that weakens its zwitterionic nature. From pMPC onward, the zwitterionic nature becomes pronounced. In the case of pMPC, the highest number of directly adsorbed water molecules per monomer, the second-highest water adsorption energy, and the highest Bader charge transfer to water molecules indicate strong polymer–water interactions. However, it exhibits the weakest individual interaction strength among the studied polymers, as shown by the longest polymer–water bonds and lowest -ICOHP value. This is likely because the anionic groups form hydrogen bonds with more water molecules, distributing the interaction across multiple sites and weakening each bond. Therefore, although pMPC directly interacts with the largest number of water molecules, these interactions are relatively weak due to the reduced average polymer–water bond strength.

For pMPC+1 and pMPC+2, both polymers adsorb a similar number of water molecules and exhibit the highest and second-highest adsorption energies, along with the second-highest Bader charge transfer. Their short polymer–water bond distances and relatively high -ICOHP values confirm strong interactions, reflecting an optimal balance between side-chain flexibility and crumpling that enables direct binding to a significant number of water molecules with high interaction strength. In contrast, pMPC+3 shows lower adsorption energy and Bader charge transfer to water compared to pMPC, pMPC+1, and pMPC+2. Despite this, it exhibits the strongest individual polymer–water interactions, as reflected by the shortest bond lengths and the highest -ICOHP values. The lower overall adsorption and charge transfer arise from fewer direct water interactions, as side-chain crumpling limits access to anionic sites. The strong bond strength is due to the localized point-charge character of unfolded anionic groups, a result of the longest $–CH_2–$ spacing. Thus, increased spacing strengthens individual bonds but promotes loop-like folding, reducing the number of accessible sites and overall water interaction. A key observation from the present study is that the Bader charge transfer does not directly follow the trend observed in the -ICOHP analysis. This discrepancy arises because both quantities are strongly influenced by the total number of directly adsorbed water molecules. Specifically, a higher number of direct water contacts leads to greater overall charge transfer. However, this simultaneously results in weaker individual hydrogen bonds. When the anionic groups interact with multiple water molecules at the same time, the interactions become more delocalized and distributed over several sites, thereby reducing the strength of each individual hydrogen bond as reflected in -ICOHP calculations.

We further analyzed the structural features of water after adsorption by comparing the OH bond lengths, HOH angles, and water–water hydrogen bond distances with those of ice-Ih, ice-10H_2O, and ice-prism configurations. These deviations in molecular geometry and intermolecular interactions provide insight into the transition from liquid-like to ice-like water structures. Fig. S1 highlights the variations in water's structural parameters relative to these ice phases, while Table S1 reports the ice similarity scores for different materials with respect to ice-Ih, illustrating how polymeric environments influence the water structure and behavior.

All the five zwitterionic polymers studied exhibit very low overall ice similarity (<11.0%), with the largest contribution arising from the HOH angle similarity. This suggests that polymer environments perturb the water HOH angle more significantly than the OH bond lengths. Moreover, the calculated similarity scores remain consistently low across all polymers with only minimal variation, likely due to water deformation induced by polymer–water interactions. Therefore, ice similarity scores may not provide a reliable metric for ranking anti-icing performance in this context. This limitation arises from the restricted system size used in the present DFT model and could be addressed through larger-scale MD simulations, which would also capture polymer conformational effects not considered here. To further probe polymer–ice interactions, in the following section we examine their interactions with an ice-10H_2O cluster.

Polymer interactions with ice

In this section, we examined the interactions of an ice-10H_2O cluster with the five zwitterionic polymers to investigate their anti-icing ability. The optimized structures (Fig. 6a) reveal that, in most cases, the hydrogen bonds between neighboring H_2O molecules in the ice cluster break, enabling the water molecules to interact directly with the anionic groups of the polymers. To quantify these interactions, we calculated the adsorption energy (Fig. 6b), formation energy (Fig. 6c), and the deformation of the ice cluster after adsorption from its ideal structure using the root mean square deviation (RMSD) value (Fig. 6d).

The adsorption energy analysis shows that pMPC exhibits the most negative value, followed by pMPC+2 and pMPC+3, then pMPC+1, and finally pMPC-1 with the least negative value. In contrast, the formation energy analysis indicates that pMPC+1 has the most positive value, suggesting that the formation of an ice cluster in its first hydration layer is energetically unfavorable. pMPC+2 and pMPC+3 also exhibit positive formation energies, nearly equal in magnitude but less positive than pMPC+1. For pMPC-1 and pMPC, although the average formation energy is positive, one of the three examined models exhibits a slightly negative value. Compared to adsorption energy, the formation energy is a more reliable metric because the loss of structural integrity in the ice cluster causes its upper layers to behave more like liquid water after adsorption. As a result, a higher adsorption energy does not necessarily indicate a stronger interaction with the ice cluster. Based on the formation energy, the polymers can be ranked in terms of their reluctance to form ice as follows: pMPC+1 > pMPC+2 ≈ pMPC+3 > pMPC > pMPC-1. Analysis of cluster deformation reveals that pMPC+1 exhibits the highest RMSD value (>0.4), indicating the greatest structural distortion of the ice cluster upon adsorption. This observation aligns with the formation

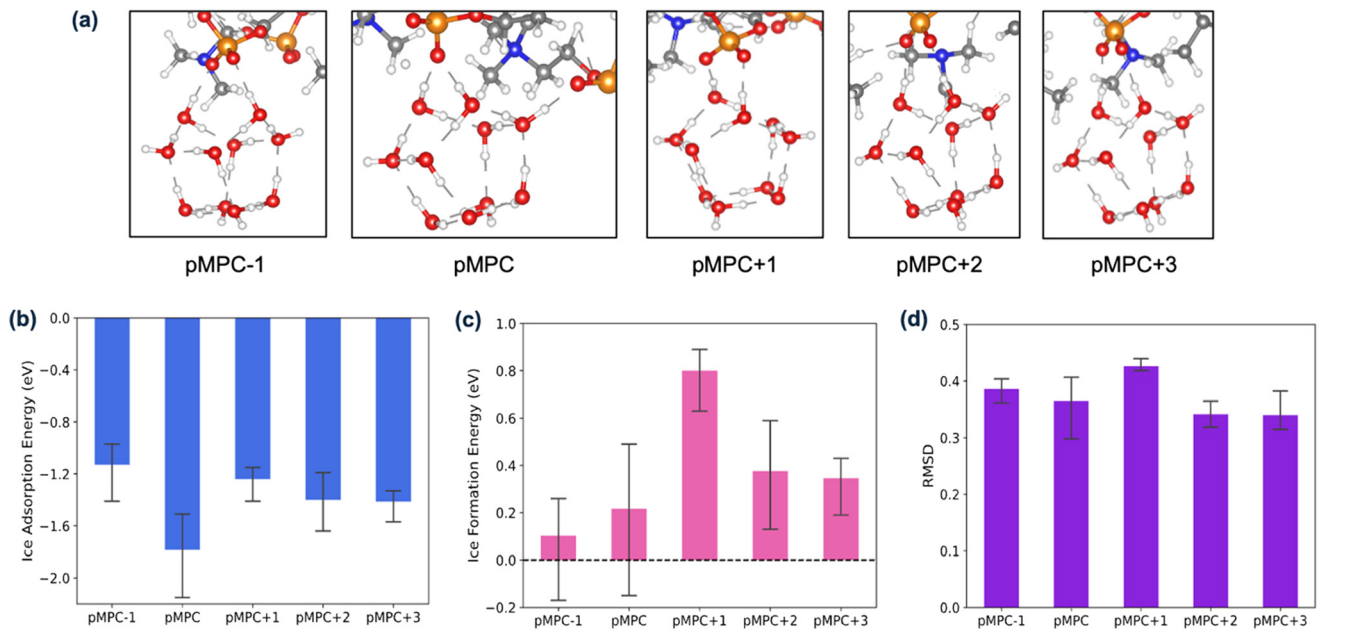

Fig. 6 (a) Optimized molecular structures of the ice cluster on all five polymers, where the dashed–dotted line indicates hydrogen bonds, (b) calculated adsorption energy (eV) of the 10-H_2O ice cluster on the polymer, (c) formation energy (eV) from liquid water molecules into the ice cluster, and (d) RMSD values (Å) quantifying structural variability.

energy results and further suggests that the ice clusters undergo deformation, behaving more like liquid water and effectively forming a self-lubricating interfacial layer. For the other four zwitterionic polymers, the observed RMSD value varies between 0.3 and 0.4, indicating moderate but noticeable structural perturbation. It should be noted that quantitative formation energies may depend on the specific ice model employed. In our previous work,[18] polymer–ice interactions were examined using multiple ice representations, including the ice-prism ($6H_2O$) cluster, ice-$10H_2O$ cluster, and the ice(001) surface. While absolute energies varied across models, the qualitative relationship between interfacial deformation and ice-formation tendency remained consistent. Accordingly, in the present study, we employ the ice-$10H_2O$ cluster as a computationally efficient model to capture local polymer–ice interactions, while acknowledging that larger clusters or extended surfaces may lead to quantitative variations.

Here, it is important to note that the present modelling approach has certain limitations. In reality, since the zwitterionic polymers exhibit good hydration behavior, ice formation would occur on the adsorbed water layer, a scenario that our current study cannot capture due to computational constraints. However, the formation energy calculation, which reflects the impact of the polymer on the transformation of liquid water to ice, provides a qualitative measure for assessing the anti-icing capability. Taken together, all three analyses indicate that pMPC+1 exhibits the strongest resistance to ice formation, making it the most promising anti-icing candidate. The positive formation energies and substantial ice cluster deformation observed for pMPC+2 and pMPC+3 also point toward weaker polymer–ice interactions.

Considering all hydration analysis results, it can be concluded that pMPC interacts with the largest number of water molecules, but through weaker individual interactions. In contrast, pMPC+3 forms the strongest polymer–water interactions, yet engages with fewer water molecules. pMPC+1 and pMPC+2 strike a balance between these two extremes, combining strong interactions with a relatively high number of direct water contacts. Therefore, among all the polymers studied, pMPC+1 and pMPC+2 demonstrate the most favorable and almost comparable hydration behavior, by interacting with an optimal number of water molecules through sufficiently strong bonding. Overall, in terms of hydration, the studied zwitterionic polymers can be ranked as: pMPC+1 $\approx$ pMPC+2 $>$ pMPC $>$ pMPC+3 $>$ pMPC-1. Consistently, ice interaction analysis shows that pMPC+1 exhibits the highest resistance to ice formation, as indicated by the most positive formation energy and the largest ice cluster deformation.

Although this study focuses on pMPC, the spacer-length effect identified here is likely transferable to other zwitterionic polymers. The governing factors—charge separation distance, dipole orientation, hydrogen-bond accessibility, and side-chain flexibility—are common structural descriptors across sulfobetaine, carboxybetaine, and phosphorylcholine systems. While quantitative energies may vary with the ionic chemistry and backbone structure, spacer-dependent modulation of interfacial hydration likely represents a broader molecular design principle. Future work could address current limitations through classical MD simulations, which can better capture polymer conformational flexibility, dynamic hydration behavior, and long-range water structuring. Although the present model employs a short oligomer, the dominant interactions governing hydration and ice resistance are primarily short-range and electronic in nature. Nonetheless, increasing polymerization degree may influence collective conformations and hydration-layer continuity, potentially affecting quantitative thermodynamics. Complementary MD studies and experimental synthesis of polymers with varied spacer lengths and molecular weights are underway to further validate and extend these findings.

Conclusion

This study systematically investigates how variations in the $-CH_2-$ spacer length influence the hydration and anti-icing behavior of zwitterionic polymers (pMPC-1, pMPC, pMPC+1, pMPC+2, and pMPC+3) using DFT calculations. The electronic structure analysis reveals minimal differences in HOMO energies and dipole moments (except for pMPC-1), while DOS results show an increase in the number of occupied states near the Fermi level with longer spacers; however, these electronic features alone do not clearly distinguish hydration performance. Structural optimization of polymer–water geometries reveals that pMPC binds the most water molecules but with the weakest interactions, whereas pMPC+3 forms the strongest bonds yet fewer water contacts due to the reduced water-accessible area caused by side-chain crumpling. Based on the adsorption energy per water molecule, Bader charge, and -ICOHP analyses, pMPC+1 and pMPC+2 demonstrate the most favorable hydration, balancing strong binding with an optimal number of water interactions.

Interaction analysis with ice clusters reveals that pMPC+1 induces the greatest deformation of the ice clusters, resulting in positive formation energy from water to ice clusters. However, within the limits of the current modeling framework, a clear ranking of the remaining polymers in terms of anti-icing performance cannot be established. Overall, the analyses indicate that pMPC+1 and pMPC+2 exhibit optimal hydration behavior, with pMPC+1 demonstrating the best anti-icing performance. These results identify three- and four-carbon spacers as optimal for achieving enhanced hydration, with the three-carbon spacer offering the best balance between hydration and anti-icing performance. These results align with the findings of Chen *et al.*,[20] who reported that a three-carbon spacer provides optimal charge separation and hydrophilicity for SB. Collectively, this study provides valuable molecular-level

insights for designing zwitterionic polymer coatings with optimized spacer lengths for advanced anti-icing applications.

Methods

In this study, we employed the Vienna *Ab Initio* Simulation Package (VASP)[32–34] to perform non-spin-polarized plane-wave DFT calculations. The core-valence interactions were treated using the projector-augmented wave (PAW) method,[35,36] and the electron exchange–correlation was described using the generalized gradient approximation (GGA) with the Perdew–Burke–Ernzerhof (PBE) functional.[37] Dispersion interactions were incorporated *via* Grimme's PBE-D3 correction with the Becke–Johnson damping function.[38] A kinetic energy cutoff of 400 eV was applied, and Brillouin-zone integrations were performed using Gaussian smearing with a width of 0.03 eV. The atomic structures were optimized using the conjugate-gradient method with convergence criteria of 10^{-6} eV for energy and 0.01 eV Å^{-1} for forces.

For the electronic and chemical property calculations of monomers in the gas phase, we used the Gaussian16 software package.[39] These calculations employed Becke's three-parameter hybrid functional (B3LYP)[40] with the Pople-type triple-ζ 6-311++G(d,p) basis set,[41] which incorporates diffuse functions on all atoms and polarization functions on both heavy atoms and hydrogens.

To model hydration and ice interactions, we employed one-dimensional periodic models of polymer chains containing four monomer units, with vacuum spacing introduced to prevent interactions between periodic replicas. The polymer backbone was defined along the *x*-axis. The monomeric units and corresponding three-dimensional periodic structures for each polymer are shown in Fig. 1. To introduce the hydrated environment, the simulation cells were filled with 80 H_2O molecules, giving an overall density of approximately 0.96 g cm^{-3}. To capture variability in water configurations around the polymer, three independent models were generated for each system with 80 randomly distributed water molecules using the Packmol package.[42] All dry and hydrated models were fully optimized to their ground-state geometries prior to morphological and bonding analyses. To quantify the interaction strength, we calculated water adsorption energies using the following equation:

$$E_{ads} = (E_{poly+adsorbate} - E_{poly} - n \times E_{adsorbate})/n \quad (1)$$

where E_{ads} is the adsorption energy per H_2O molecule, $E_{poly+adsorbate}$ is the total energy of the polymer with the adsorbate (H_2O molecules or ice cluster), E_{poly} is the energy of the dry polymer chain, and $E_{adsorbate}$ is the energy of a free water molecule or ice cluster. n corresponds to the number of water molecules per simulation cell or equals 1 in the case of ice cluster. A negative adsorption energy indicates an attractive interaction between the polymer and the adsorbate. More negative adsorption energies signify stronger polymer–water interactions, corresponding to higher hydration capability. To ensure consistent comparison across different polymer systems, the number of water molecules (n) was fixed at 80. This choice, together with the selected simulation cell sizes, ensures that most water molecules remain within the interaction range of the polymers, specifically within the first and second hydration shells. To also study the polymer–ice cluster interaction, three different models were investigated, each with the ice cluster positioned differently with respect to the polymers. Along with adsorption energy calculations, we also calculated ice cluster formation energy using the following equation:

$$E_{form} = E^{ice}_{nH_2O} - E^{liquid}_{nH_2O} \quad (2)$$

where E_{form} is the formation energy, which is calculated as the energy difference between the system with an nH_2O ice cluster adsorbed on the polymer and the corresponding system with the same number of liquid-like water molecules adsorbed. Here, $E^{liquid}_{nH_2O}$ is the total energy of the polymer with n adsorbed water molecules and $E^{ice}_{nH_2O}$ is the total energy of the system with the adsorbed ice cluster. This calculation provides insight into the likelihood of freezing, where a strongly bonded dynamic hydration layer is less likely to transition into ice.

Furthermore, to characterize the electronic structure, we calculated the electrophilicity and electronegativity of each zwitterionic monomer.[43] We also analyzed the electron density of states (DOS) for the dry polymer models, providing a quantitative measure of the state distribution across specific energy ranges. We further calculated the Bader atomic charges on the adsorbed H_2O molecules in the hydrated polymer models to probe the nature of polymer–water interactions.[44–46] The Bader electron population of an atom (Q^{Bader}_A) is calculated as the integral of the electron density [$\rho(r)$] over the atomic basin (Ω_A):

$$Q^{Bader}_A = \int_{\Omega_A} \rho(r) dr \quad (3)$$

In addition, to obtain deeper insight into the bonding characteristics between the polymer and adsorbed H_2O molecules, we performed bonding analyses using the crystal orbital Hamilton population (COHP) method,[47] as implemented in the LOBSTER code.

Author contributions

Tamalika Ash: methodology, software, formal analysis, validation, writing – original draft and review & editing. Sara A. Tolba: validation and writing – review & editing. Wenjie Xia: conceptualization, supervision, project administration, funding acquisition, resources, and writing – review & editing.

Conflicts of interest

There are no conflicts to declare.

Data availability

All data that support the findings of this study are included within the article. Additional data are available from the authors upon reasonable request.

Supplementary information (SI): the SI includes additional analyses of water–polymer interactions and ice similarity metrics. See DOI: https://doi.org/10.1039/d6me00015k.

Acknowledgements

The authors acknowledge the support from the U.S. Office of Naval Research (ONR) (Award No. N00014-22-1-2129 and N00014-24-1-2011). This work used the resources of the Center for Computationally Assisted Science and Technology (CCAST) at NDSU, which were made possible in part by the NSF MRI program (Award No. 2019077).

References

1 M. Farzaneh, C. Volat and A. Leblond, *Atmospheric Icing of Power Networks*, Springer, Dordrecht, 2008, pp. 229–268.
2 C. C. Ryerson, *Cold Reg. Sci. Technol.*, 2011, **65**, 97–110.
3 O. Parent and A. Ilinca, *Cold Reg. Sci. Technol.*, 2011, **65**, 88–96.
4 A. G. Kraj and E. L. Bibeau, *Renewable Energy*, 2010, **35**, 966–972.
5 J. Xiao and S. Chaudhuri, *Langmuir*, 2012, **28**, 4434–4446.
6 S. Jung, M. K. Tiwari, N. V. Doan and D. Poulikakos, *Nat. Commun.*, 2012, **3**, 615.
7 L. Fay and X. Shi, *Water, Air, Soil Pollut.*, 2012, **223**, 2751–2770.
8 J. Ayres, W. H. Simendinger and C. M. Balik, *J. Coat. Technol. Res.*, 2007, **4**, 463–471.
9 J. Ayres, W. H. Simendinger and C. M. Balik, *J. Coat. Technol. Res.*, 2007, **4**, 473–481.
10 R. Carriveau, A. Edrisy, P. Cadieux and R. Mailloux, *J. Adhes. Sci. Technol.*, 2012, **26**, 447–461.
11 J. Lv, Y. Song, L. Jiang and J. Wang, *ACS Nano*, 2014, **8**, 3152–3169.
12 H. Yang, C. Ma, K. Li, K. Liu, M. Loznik, R. Teeuwen, J. C. M. van Hest, X. Zhou, A. Herrmann and J. Wang, *Adv. Mater.*, 2016, **28**, 5008–5012.
13 A. Abdelmonem, E. H. G. Backus and M. Bonn, *J. Phys. Chem. C*, 2018, **122**, 24760–24764.
14 D. Ehre, E. Lavert, M. Lahav and I. Lubomirsky, *Science*, 2010, **327**, 672–675.
15 S. Bai, X. Li, R. Zhang, C. Li, K. Zhu, P. Sun, Y. Zhao, L. Ren and X. Yuan, *Chem. Eng. J.*, 2019, **357**, 667–677.
16 Z. Chen, *Langmuir*, 2022, **38**, 4483–4489.
17 X. Song, J. Man, Y. Qiu, J. Wang, R. Li, Y. Zhang, G. Cui, J. Li, J. Li and Y. Chen, *ACS Appl. Mater. Interfaces*, 2024, **16**, 17145–17162.
18 S. A. Tolba, T. Ash and W. Xia, *J. Mater. Chem. A*, 2025, **13**, 39065–39076.
19 P. Sarker, T. Lu, D. Liu, G. Wu, H. Chen, M. S. J. Sajib, S. Jiang, Z. Chen and T. Wei, *Chem. Sci.*, 2023, **14**, 7500–7511.
20 M. Chen, J. Yin and H. Wu, *Langmuir*, 2025, **41**, 822–831.
21 B. Liang, G. Zhang, Z. Zhong, Y. Huang and Z. Su, *Langmuir*, 2019, **35**, 1294–1301.
22 Q. Shao and S. Jiang, *Adv. Mater.*, 2015, **27**, 15–26.
23 K. Ishihara, N. P. Ziats, B. P. Tierney, N. Nakabayashi and J. M. Anderson, *J. Biomed. Mater. Res.*, 1991, **25**, 1397–1407.
24 Y. Zhang, Y. Liu, B. Ren, D. Zhang, S. Xie, Y. Chang, J. Yang, J. Wu, L. Xu and J. Zheng, *J. Phys. D: Appl. Phys.*, 2019, **52**, 403001.
25 S. A. Tolba and W. Xia, *Mol. Syst. Des. Eng.*, 2023, **8**, 1040–1048.
26 W. Feng, J. Brash and S. Zhu, *J. Polym. Sci., Part A: Polym. Chem.*, 2004, **42**, 2931–2942.
27 T. Morisaku, J. Watanabe, T. Konno, M. Takai and K. Ishihara, *Polymer*, 2008, **49**, 4652–4657.
28 K. Ishihara, M. Mu, T. Konno, Y. Inoue and K. Fukazawa, *J. Biomater. Sci., Polym. Ed.*, 2017, **28**, 884–899.
29 M. Takahashi, S. Chen, H. Matsui, N. Morimoto and Y. Ikemoto, *Sci. Rep.*, 2022, **12**, 20393.
30 X. Qin, J. Fang, A. A. Chen, P. Sarker, M. S. J. Sajib, M. J. Uline and T. Wei, *Langmuir*, 2025, **41**, 1005–1012.
31 P. Sarker, G. T. Chen, M. S. J. Sajib, N. W. Jones and T. Wei, *Colloids Surf., A*, 2022, **653**, 129943.
32 G. Kresse and J. Furthmüller, *Comput. Mater. Sci.*, 1996, **6**, 15–50.
33 G. Kresse and J. Furthmüller, *Phys. Rev. B: Condens. Matter Mater. Phys.*, 1996, **54**, 11169.
34 G. Kresse and J. Hafner, *Phys. Rev. B: Condens. Matter Mater. Phys.*, 1993, **47**, 558.
35 P. E. Blöchl, *Phys. Rev. B: Condens. Matter Mater. Phys.*, 1994, **50**, 17953.
36 G. Kresse and D. Joubert, *Phys. Rev. B: Condens. Matter Mater. Phys.*, 1999, **59**, 1758.
37 J. P. Perdew, K. Burke and M. Ernzerhof, *Phys. Rev. Lett.*, 1996, **77**, 3865.
38 S. Grimme, J. Antony, S. Ehrlich and H. Krieg, *J. Chem. Phys.*, 2010, **132**, 154104.
39 M. J. Frisch, G. W. Trucks, H. B. Schlegel, G. E. Scuseria, M. A. Robb, J. R. Cheeseman, G. Scalmani, V. Barone, G. A. Petersson, H. Nakatsuji, X. Li, M. Caricato, A. V. Marenich, J. Bloino, B. G. Janesko, R. Gomperts, B. Mennucci, H. P. Hratchian, J. V. Ortiz, A. F. Izmaylov, J. L. Sonnenberg, D. Williams-Young, F. Ding, F. Lipparini, F. Egidi, J. Goings, B. Peng, A. Petrone, T. Henderson, D. Ranasinghe, V. G. Zakrzewski, J. Gao, N. Rega, G. Zheng, W. Liang, M. Hada, M. Ehara, K. Toyota, R. Fukuda, J. Hasegawa, M. Ishida, T. Nakajima, Y. Honda, O. Kitao, H. Nakai, T. Vreven, K. Throssell, J. A. Montgomery Jr., J. E. Peralta, F. Ogliaro, M. J. Bearpark, J. J. Heyd, E. N. Brothers, K. N. Kudin, V. N. Staroverov, T. A. Keith, R. Kobayashi, J. Normand, K. Raghavachari, A. P. Rendell, J. C. Burant, S. S. Iyengar, J. Tomasi, M. Cossi, J. M.

Millam, M. Klene, C. Adamo, R. Cammi, J. W. Ochterski, R. L. Martin, K. Morokuma, O. Farkas, J. B. Foresman and D. J. Fox, *Gaussian 16*, Revision C.01, Gaussian, Inc., Wallingford CT, 2016.

40 A. D. Becke, *J. Chem. Phys.*, 1993, **98**, 1372–1377.

41 L. A. Curtiss, M. P. McGrath, J.-P. Blaudeau, N. E. Davis, R. C. Binning and L. Radom, *J. Chem. Phys.*, 1995, **103**, 6104–6113.

42 L. Martínez, R. Andrade, E. G. Birgin and J. M. Martínez, *J. Comput. Chem.*, 2009, **30**, 2157–2164.

43 C.-G. Zhan, J. A. Nichols and D. A. Dixon, *J. Phys. Chem. A*, 2003, **107**, 4184–4195.

44 G. Henkelman, A. Arnaldsson and H. Jónsson, *Comput. Mater. Sci.*, 2006, **36**, 354–360.

45 W. Tang, E. Sanville and G. Henkelman, *J. Phys.: Condens. Matter*, 2009, **21**, 084204.

46 E. Sanville, S. D. Kenny, R. Smith and G. Henkelman, *J. Comput. Chem.*, 2007, **28**, 899–908.

47 S. Maintz, V. L. Deringer, A. L. Tchougréeff and R. Dronskowski, *J. Comput. Chem.*, 2016, **37**, 1030–1035.